Serotonergic and dopaminergic neurons in the dorsal raphe are differentially altered in a mouse model for Parkinson's disease.

Laura Boi[1†], Yvonne Johansson[2†], R Tonini[3] ,R Moratalla[4,5], Gilberto Fisone[1‡*], Gilad Silberberg[1‡*].

1 Department of Neuroscience, Karolinska Institutet, Stockholm 17177, Sweden.
2 Sainsbury Wellcome Centre for Neural Circuits and Behaviour, University College London, London, UK.
3 Neuromodulation of Cortical and Subcortical Circuits Laboratory, Istituto Italiano di Tecnologia, Genova, Italy.
4 Cajal Institute, Spanish National Research Council (CSIC), Madrid, Spain.
5 CIBERNED, Instituto de Salud Carlos III, Madrid, Spain.

† These authors contributed equally to this work
‡ These authors contributed equally to this work
* Corresponding author

Abstract

Parkinson's disease (PD) is characterized by motor impairments caused by degeneration of dopamine neurons in the substantia nigra pars compacta. In addition to these symptoms, PD patients often suffer from non-motor co-morbidities including sleep and psychiatric disturbances, which are thought to depend on concomitant alterations of serotonergic and noradrenergic transmission. A primary locus of serotonergic neurons is the dorsal raphe nucleus (DRN), providing brain-wide serotonergic input. Here, we identified electrophysiological and morphological parameters to classify serotonergic and dopaminergic neurons in the murine DRN under control conditions and in a PD model, following striatal injection of the catecholamine toxin, 6-hydroxydopamine (6-OHDA). Electrical and morphological properties of both neuronal populations were altered by 6-OHDA. In serotonergic neurons, most changes were reversed when 6-OHDA was injected in combination with desipramine, a noradrenaline reuptake inhibitor, protecting the noradrenergic terminals. Our results show that the depletion of both noradrenaline and dopamine in the 6-OHDA mouse model causes changes in the DRN neural circuitry.

Introduction

Parkinson's Disease (PD) is a frequent neurodegenerative disorder characterized by the progressive loss of dopaminergic neurons in the nigrostriatal pathway, leading to bradykinesia, tremor, rigidity, and postural instability [1, 2]. These cardinal motor symptoms are typically addressed by administration of dopaminergic drugs or by deep brain stimulation. PD patients also experience non-motor symptoms including sleep, affective, and cognitive dysfunctions often preceding the motor disabilities [3, 4]. These comorbidities are in large part refractory to current PD treatments and are thought to be caused by neurodegenerative processes occurring in concomitance to the loss of midbrain dopaminergic neurons. However, the pathology underlying non-motor symptoms remains poorly understood.

Post-mortem studies in PD patients provided first insights into the brain areas which might be involved in the etiology of non-motor dysfunctions in PD. Besides the profound degeneration of the substantia nigra pars compacta (SNc), these studies found cell loss and reduced neurotransmitter release in other monoaminergic brain regions, including the dorsal and median raphe nuclei (DRN and MRN, respectively), and the locus coeruleus (LC) [1, 5-8]. The DRN constitutes the main source of serotonin in the brain with serotonergic cells ($DRN^{5\text{-}HT}$) accounting for 30-50% of its neurons [9]. $DRN^{5\text{-}HT}$ neurons have been implicated in numerous neuropsychiatric diseases, rendering them a potential neural substrate for non-motor symptoms in PD. In fact, several studies have shown that serotonergic markers and transmitter levels are altered in Parkinson patients as well as in non-human primate and rodent models of PD [10-17]. Notably, alterations in the serotonergic system have also been related to non-motor comorbidities in PD [18, 19]. Yet, functional investigations of $DRN^{5\text{-}HT}$ in rodent models of PD have led to conflicting results showing both increased and decreased activity in $DRN^{5\text{-}HT}$ neurons themselves as well as in their downstream targets [20-22]. Besides the serotonergic neurons, the DRN comprises other neuronal populations, including a group of dopamine neurons (DRN^{DA}), in which Lewy bodies have been found in PD patients [6]. DRN^{DA} neurons have been linked to the regulation of pain, motivational processes, incentive memory, wakefulness and sleep-wake transitions [23-27], but their ultimate behavioral significance is yet to be elucidated [28-32]. In addition, the physiology and pathophysiology of DRN^{DA} neurons in PD remains elusive. The sparsity of research on DRN^{DA} neurons is likely due to the technical challenges associated with targeting this population among the diverse cell types in the DRN and adjacent structures (e.g., retrorubral field, periaqueductal grey and LC), which often co-express signature genes, hampering their molecular identification and region-specific manipulations with cre driver lines [9, 33-36].

Recently, this issue has been addressed by Pinto and colleagues who showed that DRN^{DA} neurons are most faithfully labelled in transgenic mice in which the expression of cre is linked to the dopamine transporter (DAT-cre) [34]. Previously, the membrane properties of DRN^{DA} neurons have only been addressed in mice in which DRN^{DA} neurons were identified based on the expression of the transcription factor Pitx3 or the enzyme tyrosine hydroxylase (TH) [33]. In Pitx3-GFP mice, about 70% of GFP-positive neurons are TH-positive as shown by immunohistochemistry. Moreover, 40% of TH-positive neurons in the DRN are not labelled in these mice, suggesting that this line targets a subpopulation of DRN^{DA} neurons [33]. The widely used TH-cre reporter line has been found to show ectopic expression of cre in non-dopaminergic neurons, probably caused by a transient developmental expression of TH [37, 38]. In addition, the TH-cre line also labels noradrenergic neurons in the neighboring LC [37], which produces most of the noradrenaline (NA) in the brain and is involved in mood control, cognition, and sleep regulation [39]. The large overlap of functions ascribed to the LC and DRN is thought to result from the complex reciprocal synaptic connections between these two brain areas: notably, the LC provides noradrenergic input to the DRN [40, 41] and also receives input from $DRN^{5\text{-}HT}$ neurons [42-44].

Here, we used ex vivo whole-cell patch clamp recordings and morphological reconstructions to characterize the electrophysiological and morphological properties of DRN^{DA} and $DRN^{5\text{-}HT}$ neurons in wild type and DAT-tdTomato mice. Moreover, we studied the impact of catecholamine depletion on DRN^{DA} and $DRN^{5\text{-}HT}$ populations in the 6-OHDA toxin model of PD.

81 # Results

82 ## DRN^{DA} and $DRN^{5\text{-}HT}$ neurons are electrophysiologically distinct cell-types

83 To investigate the electrophysiological and morphological profile of DRN^{DA} neurons and to compare it to
84 $DRN^{5\text{-}HT}$ neurons, we performed whole-cell patch clamp recordings in coronal slices of adult wild type and
85 DAT-cre mice crossed with tdTomato reporter mice (**Figure 1**A). All neurons were filled with neurobiotin
86 and Alexa488 while recording. Alexa488 allowed us to take snapshots of recorded neurons at different time
87 points, thus facilitating the topographical registration of recorded neurons to the post-hoc stained slices
88 (Suppl. Figure 1). Using this approach, we obtained complete sets of electrophysiological and morphological
89 data from 75 neurons in the DRN. Cells were identified as $DRN^{5\text{-}HT}$ or DRN^{DA} neurons based on tryptophan
90 hydroxylase (TPH) or TH immunoreactivity, respectively (Figure 1A-D). None of the recorded neurons was
91 positive for both TPH and TH (n = 0/412). During the recordings, we used a series of depolarizing and
92 hyperpolarizing current steps and ramps that allowed us to characterize active and passive membrane
93 properties in detail (Figure 1E – G). Based on the electrophysiological data, we first tested possible
94 differences between TH-positive neurons recorded in wild-type mice and tdTomato-positive neurons
95 recorded in DAT-tdTomato mice. We found no differences between these two groups (n = 13 TH-positive
96 vs n = 30 tdTomato-positive neurons, Suppl. Figure 2A) and neither within the subset of tdTomato-positive
97 neurons when comparing TH-positive to TH-negative neurons (n = 25 TH-positive vs n = 5 TH-negative
98 neurons, Suppl. Figure 2A–E). Out of 114 tdTomato-positive neurons only one cell displayed a different
99 electrophysiological profile than all other DRN^{DA} neurons, suggesting a false-positive rate of 0.8%. That
100 neuron was TH-negative and displayed profoundly distinct intrinsic properties, and was therefore excluded
101 (Suppl. Figure 2F, G). Taken together, the electrophysiological results support the use of the DAT-tdTomato
102 mouse line when studying DRN^{DA} neurons and data from both mouse lines were pooled. Recordings of
103 DRN^{DA} neurons showed that they share several properties characteristic of other dopaminergic populations
104 located in the SNc and the ventral tegmental area, such as a slowly ramping membrane potential during
105 constant current injections giving rise to delayed spiking and postinhibitory hypoexcitability (Figure 1E; [45,
106 46]). Moreover, like other dopaminergic populations in the midbrain, most DRN^{DA} neurons displayed
107 rebound oscillations and the vast majority of cells expressed sag currents (Figure 1E, F). When comparing
108 the electrophysiological properties of DRN^{DA} to $DRN^{5\text{-}HT}$ neurons, we observed numerous differences
109 between these two cell types, but here we focus on the five most significant ones. While $DRN^{5\text{-}HT}$ neurons
110 spike with short delays in response to current steps and maintain a relatively constant action potential (AP)
111 amplitude, DRN^{DA} neurons display a longer delay to the first spike and the amplitude of subsequent action
112 potentials drops (Figure 1F-I). Additionally, the action potentials of $DRN^{5\text{-}HT}$ neurons rise faster, while their
113 afterhyperpolarization (AHP) is longer compared to DRN^{DA} neurons (Figure 1H, I). Lastly, the capacitance of
114 $DRN^{5\text{-}HT}$ neurons is significantly larger than in DRN^{DA} neurons (Figure 1I).

115 Next, we tested if DRN^{DA} neurons can be distinguished from $DRN^{5\text{-}HT}$ neurons based on these five
116 electrophysiological parameters. To this end, we standardized the data and ran a principal component
117 analysis (PCA) including all $DRN^{5\text{-}HT}$ neurons (i. e. all TPH-positive), all TH-positive neurons recorded in wild-
118 type mice and all tdTomato-positive cells recorded in DAT-tdTomato mice (except for one outlier shown in
119 Suppl. Figure 2F, G). Plotting the first two principal components (PC) showed two separate clusters (Figure
120 1J, insert). Unsupervised hierarchical cluster analysis based on PC1 and PC2 revealed the same two major
121 clusters and potential subclusters (Figure 1J). Mapping the molecular identity of the cells onto the

122 dendrogram revealed the separation of $DRN^{5\text{-}HT}$ and DRN^{DA} neurons, while there was no branching
123 according to mouse line (wild type vs. DAT-tdTomato), further corroborating the validity of DAT-tdTomato
124 mice as a marker for DRN^{DA} neurons. Overall, these data suggest that electrophysiological parameters
125 themselves are sufficient to distinguish between $DRN^{5\text{-}HT}$ and DRN^{DA} neurons.
126 In addition to DRN^{DA} and $DRN^{5\text{-}HT}$ the DRN contains an unknown number of cell types and 47 out of 120
127 recorded neurons were neither TH-positive, nor TPH-positive and did not express tdTomato. To test
128 whether DRN^{DA} can also be distinguished from those populations based on their electrophysiological
129 profile, we ran a PCA on 20 standardized parameters and used the first three PCAs for unsupervised
130 hierarchical clustering (Suppl. Figure 3). Our analysis suggests that there might be four major
131 electrophysiological cell types in the DRN. In contrast to DRN^{DA} and $DRN^{5\text{-}HT}$ neurons, a large proportion of
132 the remaining cells showed rebound spiking and biphasic AHPs, resembling the profiles of local
133 interneurons in other brain areas (Suppl. Figure 3D, E). Interestingly, the clustering also indicated that three
134 TH- and tdTomato-negative neurons belonged to the DRN^{DA} neurons and further analysis showed that they
135 were indistinguishable from molecularly identified DRN^{DA} neurons (Suppl. Figure 3C, F). These findings
136 indicate that clustering can be used to identify neurons that otherwise would have been excluded due to a
137 lack of post-hoc staining data or genetic driver lines.
138 Overall, our data show that DRN^{DA} neurons constitute an electrophysiologically distinct class of neurons in
139 the DRN expressing several hallmark properties, which are sufficient to identify them within the local DRN
140 circuitry.
141
142 **DRN^{DA} and $DRN^{5\text{-}HT}$ neurons have different morphological profiles**
143 Next, we characterized the morphological profile of $DRN^{5\text{-}HT}$ and DRN^{DA} neurons. We focused on the analysis
144 of somatic and dendritic properties since a complete reconstruction of the axonal arborization could not
145 be retrieved from the slices. The analysis of the somatic properties showed that $DRN^{5\text{-}HT}$ neurons had larger
146 cell bodies than DRN^{DA} neurons (**Figure 2**A-E), as measured in their area, perimeter, length, and width
147 (Figure 2B-E). Cell bodies also differed in shape, with DRN^{DA} neurons having more circular somata than
148 $DRN^{5\text{-}HT}$ neurons, as indicated by the circularity index (Figure 2F). Analyzing the dendritic properties, we
149 found that $DRN^{5\text{-}HT}$ neurons had four to five primary dendrites, compared to only two to three in DRN^{DA}
150 neurons (Figure 2G). Moreover, dendrites of DRN^{DA} neurons were frequently bipolar with the main primary
151 dendrites starting from opposite extremes of the soma. Both populations had relatively few bifurcations
152 (Figure 2H) but the $DRN^{5\text{-}HT}$ neurons had significantly more terminations (Figure 2I). The overall dendritic
153 length did not differ between the $DRN^{5\text{-}HT}$ and DRN^{DA} neurons: both populations had a mix of short and long
154 dendrites (Figure 2L). These data suggest that $DRN^{5\text{-}HT}$ neurons have denser dendritic arborization than
155 DRN^{DA} neurons, mostly due to larger numbers of primary dendrites.
156 Altogether, our results show that $DRN^{5\text{-}HT}$ and DRN^{DA} neurons have distinct morphological properties. $DRN^{5\text{-}}$
157 ^{HT} neurons are mostly multipolar neurons, with a big and complex soma and multiple primary dendrites,
158 while DRN^{DA} neurons have smaller and more circular cell bodies with bipolar dendrites.
159
160 **DA and NA depletion distinctly affect the membrane properties of $DRN^{5\text{-}HT}$ neurons**
161 To elucidate how $DRN^{5\text{-}HT}$ and DRN^{DA} neurons might be affected in PD, we characterized these populations
162 in a mouse model of PD based on bilateral injection of the neurotoxin 6-OHDA in the dorsal striatum. This
163 approach leads to a partial lesion of catecholamine neurons, reproducing an early stage of parkinsonism in

which particularly non-motor symptoms are manifested [47]. In line with previous studies, we observed a 60-70% reduction of TH levels in the striatum (Suppl. Figure 4, [48]). Only mice meeting this criterion were included in the study. Immunostaining showed that the striatal 6-OHDA injection did not cause degeneration of $DRN^{5\text{-}HT}$ or DRN^{DA} neurons (Suppl. Figure 5).

Striatal injection of 6-OHDA has also been found to produce a partial loss of NA neurons in the LC [48]. In the present study, we determined the specific impact of NA dysfunction on the physiology of $DRN^{5\text{-}HT}$ and DRN^{DA} neurons by pre-treating a group of mice with desipramine (DMI), a selective inhibitor of noradrenaline reuptake, before injecting 6-OHDA (DMI+6-OHDA mice). We then assessed the intrinsic properties of $DRN^{5\text{-}HT}$ and DRN^{DA} neurons in Sham-lesion (Sham), 6-OHDA- and DMI+6-OHDA-treated mice. Whole-cell recordings obtained from $DRN^{5\text{-}HT}$ neurons in control mice revealed that 36% of $DRN^{5\text{-}HT}$ neurons were spontaneously active in slices and the proportion of intrinsically active neurons was similar in mice injected with 6-OHDA (control: n = 12/33 $DRN^{5\text{-}HT}$ neurons, 6-OHDA: n = 7/18 $DRN^{5\text{-}HT}$ neurons, **Figure 3**A). However, $DRN^{5\text{-}HT}$ neurons recorded in DMI+6-OHDA mice showed an increased excitability: in this condition 73% of $DRN^{5\text{-}HT}$ neurons were spontaneously active and $DRN^{5\text{-}HT}$ neurons displayed lower rheobase currents than in control and 6-OHDA mice (Figure 3A, B). Since the noradrenergic system is protected by DMI in these mice, these findings suggest that the 6-OHDA induced lesion of midbrain dopaminergic neurons evoked the increased firing of $DRN^{5\text{-}HT}$ neurons.

While the excitability of $DRN^{5\text{-}HT}$ neurons was not affected in 6-OHDA mice, we observed that their firing properties were profoundly altered: $DRN^{5\text{-}HT}$ neurons recorded in 6-OHDA mice displayed significantly smaller and shorter APs and AHPs compared to Sham mice (Figure 3C-E). Moreover, $DRN^{5\text{-}HT}$ neurons fired at higher frequencies and with shorter delays in response to current injections (Figure 3F-H). Finally, the membrane time constant of $DRN^{5\text{-}HT}$ neurons was shorter in 6-OHDA injected mice than in Sham mice (Figure 3I). Interestingly, these changes were not observed in 6-OHDA injected mice pre-treated with DMI, suggesting that the noradrenergic lesion – and not the dopaminergic lesion – underlies the changes in the firing properties of $DRN^{5\text{-}HT}$ neurons in 6-OHDA mice. Taken together, these results indicate that $DRN^{5\text{-}HT}$ neurons are affected in the 6-OHDA mouse model of PD. Specifically, lesions of the dopaminergic system increase the excitability of $DRN^{5\text{-}HT}$ neurons whereas lesions of the noradrenergic systems change the firing properties of $DRN^{5\text{-}HT}$ neurons.

6-OHDA lesion induced hypotrophy of $DRN^{5\text{-}HT}$ neurons

Morphological analysis revealed a reduced soma size of the $DRN^{5\text{-}HT}$ neurons in 6-OHDA mice, which was manifested in a decrease in area, perimeter, and major axes in comparison to control mice (**Figure 4**A-C). Moreover, the increase in the circularity of the 6-OHDA group indicated that the shape of the soma of $DRN^{5\text{-}HT}$ neurons was also altered by the lesion (Figure 4C). These modifications were not observed in DMI + 6-OHDA mice, suggesting that preserving the noradrenaline system protected the $DRN^{5\text{-}HT}$ neurons (Figure4A-C). Finally, the injection of 6-OHDA also caused a significant reduction in the number of primary dendrites of $DRN^{5\text{-}HT}$ neurons in the 6-OHDA group and a tendency to fewer termination points (Figure 4D). The number of bifurcations and the dendritic length were not affected by the lesion (Figure 4D). Globally, these results suggest that the lesion produced by 6-OHDA induces a hypotrophic phenotype in $DRN^{5\text{-}HT}$ neurons characterized by a shrinkage of the soma and a decrease in dendritic branching and that these alterations are partly NA-dependent.

206 **6-OHDA lesion affects the firing of DRN^{DA} neurons independent of NA loss**
207 Finally, we assessed whether the striatal 6-OHDA lesion affects the physiology of DRN^{DA} neurons. Whole-
208 cell patch-clamp recordings revealed that 58% of DRN^{DA} neurons are spontaneously active in slices of Sham-
209 lesion mice (**Figure 5**A). In contrast, the proportion of intrinsically active neurons increased to 77% and 78%
210 of DRN^{DA} neurons in 6-OHDA injected mice with and without pre-treatment with DMI, respectively. In line
211 with this, silent DRN^{DA} neurons recorded in DMI + 6-OHDA mice were also found to have more depolarized
212 resting membrane potentials and hence to be closer to action potential threshold (Figure 5B). Yet, active
213 DRN^{DA} neurons tended to fire at lower frequencies in all 6-OHDA mice compared to control mice.
214 In stark contrast to DRN$^{5\text{-}HT}$ neurons, the APs and AHPs of DRN^{DA} neurons were not affected in any 6-OHDA
215 mice (Figure 5C-E). In fact, we did not observe any change in the firing properties of DRN^{DA} neurons that
216 were dependent on the protection of the NA system with DMI (Figure 5). Like DRN$^{5\text{-}HT}$ neurons, DRN^{DA}
217 neurons displayed a reduction in spike latency in 6-OHDA mice, but the shortening of the delay was also
218 present in DMI+6-OHDA mice. Together, these results suggest that the electrophysiological properties of
219 DRN^{DA} neurons are affected in the 6-OHDA mouse model of PD and that these changes are primarily due
220 to the lesion of the nigrostriatal dopaminergic pathway.
221
222 **Striatal 6-OHDA injections increased soma complexity and dendritic branching in DRN^{DA} neurons**
223 The morphological analysis of DRN^{DA} neurons revealed that the striatal 6-OHDA injection caused a
224 significant reduction of the circularity from 0.82 (Sham) to 0.77 (6-OHDA) (**Figure 6**A-C), indicating
225 increased complexity of the DRN^{DA} soma. We also observed that this effect was not present in the mice
226 pre-treated with DMI (Figure 6C). The soma size was not affected by the lesion and no changes in the area,
227 perimeter, length, and width were found (Figure 6C). However, dendritic branching, as shown by the
228 increase in termination points and bifurcations in DRN^{DA} neurons was increased in 6-OHDA-injected mice,
229 but not in mice treated with a combination of DMI and 6-OHDA (Figure 6D). The number of primary
230 dendrites and the overall dendritic length were not affected by the 6-OHDA lesion (Figure 6D). Overall,
231 these data suggest that impairment of noradrenergic function caused by the striatal 6-OHDA injection
232 altered the soma shape and dendritic branching of DRN^{DA} neurons.
233

234 Discussion

235 In the present study we combine *ex vivo* whole-cell patch clamp recordings with morphological
236 reconstructions and immunohistochemistry, to show that DRN^{DA} neurons have a distinct
237 electrophysiological profile, which is sufficient to distinguish them from DRN$^{5\text{-}HT}$ neurons as well as other
238 neuron classes in the DRN. Utilizing this approach, we also reveal that, in a 6-OHDA mouse model of PD,
239 DRN$^{5\text{-}HT}$ neurons display distinct pathophysiological changes depending on the loss of dopamine and
240 noradrenaline. Notably, degeneration of noradrenergic neurons affects not only the electrical properties
241 of DRN$^{5\text{-}HT}$ neurons but also evokes hypotrophy of their cell bodies. In contrast, the loss of nigrostriatal
242 dopamine mainly affects the electrophysiological properties of DRN^{DA} neurons while concomitant loss of
243 noradrenaline alters their morphology.
244
245 We used an extensive electrophysiological characterization protocol to quantify the differences between
246 the DRN^{DA} and DRN$^{5\text{-}HT}$ populations. The electrophysiological properties agree with previous studies, such

247 as the spontaneous firing pattern seen in DRN^{DA} neurons [33], and the slow AHP of $DRN^{5\text{-}HT}$ neurons [21].
248 Standard electrophysiological parameters were used to create a classification tool, which efficiently
249 identifies $DRN^{5\text{-}HT}$ and DRN^{DA} cells, including dopamine neurons confirmed by TH staining and / or by
250 fluorescent expression in DAT-tomato mice (Figure 1). Importantly, the DRN^{DA} neurons recorded from wild-
251 type and DAT-tdTomato mice did not differ in their electrical properties, indicating that the transgene does
252 not interfere with the membrane properties of this population.
253
254 We showed that DRN^{DA} neurons share electrophysiological properties with other dopaminergic populations
255 in the midbrain [45, 46] but have electrophysiological profiles distinct from $DRN^{5\text{-}HT}$ neurons as well as other
256 neuronal populations in the DRN. Most of the parameters extracted in our characterization rely on
257 intracellular recordings of the membrane potential. However, some properties such as the spontaneous
258 firing and action potential kinetics could be useful for *in vivo* characterization, even in extracellular
259 recordings [49-51]. In addition to the $DRN^{5\text{-}HT}$ and DRN^{DA} neuronal populations, a large fraction of neurons
260 displayed electrophysiological properties that were distinct from these two groups (Suppl. Figure 3),
261 suggesting that there are other neuronal subtypes in the DRN network, such as previously reported
262 GABAergic, glutamatergic, and peptidergic neurons [9, 52-57].
263
264 In line with previous studies, the majority of $DRN^{5\text{-}HT}$ neurons were large multipolar or fusiform neurons
265 with four to five primary dendrites, very distinct from the DRN^{DA} neurons [58-60]. Very little is known about
266 the morphology of the DRN^{DA} neurons, but previous studies identified small ovoid cells in the DRN which
267 are likely to correspond to the DRN^{DA} cells [33, 61]. Out of 25 reconstructed $DRN^{5\text{-}HT}$ neurons, only one
268 displayed dendritic spines. Previous studies in rats, described the presence of dendritic spines in most $DRN^{5\text{-}}$
269 ^{HT} neurons [62]. However, the study was performed in thicker slices and the dendritic spines were scarce
270 in the primary and secondary dendrites, while they became dense in the distal dendrites, thus it is possible
271 that in our study those dendrites were not present [62].
272
273 In the present study we assessed the impact on DRN cells of a striatal bilateral 6-OHDA lesion performed
274 with or without DMI pre-treatment, which has been shown to protect the NA neurons from the 6-OHDA-
275 induced degeneration [48, 63, 64]. We found that both $DRN^{5\text{-}HT}$ and DRN^{DA} populations were affected in a
276 cell-type specific manner by the combined action of 6-OHDA on DA and NA, with $DRN^{5\text{-}HT}$ neurons being
277 particularly sensitive to changes in the noradrenergic system. Loss of SNc dopaminergic neurons alone (6-
278 OHDA + DMI) – which are known to target $DRN^{5\text{-}HT}$ neurons directly – increased the excitability and
279 spontaneous activity in $DRN^{5\text{-}HT}$ neurons [53]. This is in line with previous *ex vivo* and *in vivo* studies showing
280 that the $DRN^{5\text{-}HT}$ neurons display increased firing rates in rodents pre-treated with DMI and injected with
281 6-OHDA [21, 65] As hypothesized by Prinz et al. [21], the selective loss of midbrain DA may induce a
282 homeostatic increase in the excitability of $DRN^{5\text{-}HT}$ neurons. Our data contrast with a previous *in vivo* study
283 showing decreased firing activity in $DRN^{5\text{-}HT}$ neurons where injection of 6-OHDA was preceded by treatment
284 with DMI and fluoxetine [22]. This dissimilarity may be related to species-specific (rat vs mouse) and
285 technical (intracerebroventricular vs striatal injections, recordings performed at 10 days vs 3 weeks after
286 the 6-OHDA injection). Importantly, in the same study identification of $DRN^{5\text{-}HT}$ neurons was not
287 molecularly confirmed and the data may include other spontaneously active DRN neurons. In fact, our
288 recordings show that there are non-serotonergic neurons in the DRN, which are spontaneously active and

289 display a regular, slow firing frequency similar to DRN^{5-HT} neurons, highlighting the importance of
290 unequivocal identification of DRN cell types.
291
292 The present study shows that combined DA and NA lesioning affects DRN^{5-HT} neurons more profoundly than
293 selective loss of DA (Figure 3, 4). In mice treated with 6-OHDA only, several electrophysiological and
294 morphological properties were altered (Figure 3, 4). The time constant and AHP of DRN^{5-HT} neurons were
295 shorter and the neurons responded with higher firing frequencies to current injections than in sham. This
296 finding suggests that the pronounced AHP and long tau of these neurons may act as a "brake" limiting their
297 maximum firing frequency in control conditions and that this brake is reduced when the NA system is
298 lesioned. Future studies are needed to assess if DRN^{5-HT} in fact fire at higher rates in vivo in mice treated
299 with 6-OHDA. In contrast, such changes in DRN^{5-HT} neurons were prevented when the NA system was
300 protected by pre-treatment with DMI. These findings indicate an important role for NA as mediator of
301 changes in the activity and properties of DRN^{5-HT} neurons. The changes produced by the 6-OHDA lesion on
302 the DRN^{DA} population were less pronounced than and different from those in DRN^{5-HT} neurons. In terms of
303 electrophysiological properties, the observed changes were primarily in the DA only lesion (6-OHDA + DMI),
304 suggesting that unlike DRN^{5-HT}, DRN^{DA} neurons are affected by the loss of midbrain DA rather than the
305 accompanying changes in NA (Figure 5). Conversely, the morphological changes produced by 6-OHDA in
306 DRN^{DA} neurons appeared to require a concomitant DA and NA lesion, suggesting a stronger impact of the
307 NA modulation (Figure 6).
308
309 Our results show that DRN neurons are affected by depletion of both DA and NA, thus raising the possibility
310 that non-motor symptoms in PD are a result of the intricate organization of DA and NA neuromodulation
311 as well as the interactions between the different DRN neuronal populations. Moreover, our results highlight
312 the complex interplay between different neuromodulator systems [66], in this case NA, DA, and 5-HT in the
313 DRN. The NA system is profoundly affected in PD [1, 8], but the precise pathophysiological processes
314 resulting from loss of NA, and specifically the impact on DRN, are yet to be elucidated.
315
316 In conclusion, our study provides a quantitative description and classification scheme for two major
317 neuronal populations in the dorsal raphe nucleus, DRN^{5-HT} and DRN^{DA} neurons. We identified novel
318 electrophysiological and morphological changes in these populations in response to DA and NA depletion
319 in the basal ganglia. Considering the involvement of DRN and LC in the development of non-motor
320 comorbidities, this study provides useful insights to understand better how these areas are affected in the
321 parkinsonian condition. Moreover, our data pave the way for future experiments to characterize these
322 subpopulations in terms of receptor expression and synaptic connectivity to shed light on their functional
323 roles particularly with regard to the wide variety of non-motor symptoms observed in PD.

Methods

Experimental model details

All animal procedures were performed in accordance with the national guidelines and approved by the local ethics committee of Stockholm, Stockholms Norra djurförsöksetiska nämnd, under ethical permits to G. F. (N12148/17) and G. S. (N2020/2022). All mice (N=30) were group-housed under a 12 hr light / dark schedule and given ad libitum access to food and water. Wild-type mice ('C57BL/6J', #000664, the Jackson laboratory) and DAT-cre (Stock #006660 the Jackson laboratory) mice crossed with homozygous tdTomato reporter mice ('Ai9', stock #007909, the Jackson laboratory) were used.

6-OHDA model

Three-month old, male and female C57BL/6J or DAT-tdTomato were deeply anesthetized with Isoflurane and mounted on a stereotaxic frame (Stoelting Europe, Dublin, Ireland). To achieve a partial striatal lesion, each mouse received a bilateral injection of 1.25 µl of 6-hydroxydopamine hydrochloride (6-OHDA, (Sigma-Aldrich, 4µg/µl) or vehicle (0.9 % NaCl + Ascorbic Acid 0.02%) in the dorsolateral striatum, according to the following coordinates: anteroposterior +0.6 mm, mediolateral ± 2.2, dorsoventral -3.2 from Bregma, as previously described [47, 67]. One group of mice (referred to as DMI + 6-OHDA) was pre-treated with desipramine hydrochloride (DMI, Sigma-Aldrich, 25mg/kg i.p.) 30 minutes before the 6-OHDA infusion in order to protect the noradrenergic system [48].

Slice preparation and electrophysiology

Three weeks after the 6-OHDA injection, mice were deeply anaesthetized with isoflurane and decapitated. The brain was quickly removed and immersed in ice-cold cutting solution containing 205 mM sucrose, 10 mM glucose, 25 mM NaHCO3, 2.5 mM KCl, 1.25 mM NaH2PO4, 0.5 mM CaCl2 and 7.5 mM MgCl2. In all experiments, the brain was divided into two parts: the striatum was dissected from the anterior section for Western Blot and the posterior part was used to prepare coronal brain slices (250 um) with a Leica VT 1000S vibratome. Slices were incubated for 30-60 min at 34°C in a submerged chamber filled with artificial cerebrospinal fluid (ACSF) saturated with 95% oxygen and 5% carbon dioxide. ACSF was composed of 125 mM NaCl, 25 mM glucose, 25 mM NaHCO3, 2.5 mM KCl, 2 mM CaCl2, 1.25 mM NaH2PO4, and 1 mM MgCl2. Subsequently, slices were kept for at least 60 min at room temperature before recording.

Whole-cell patch clamp recordings were obtained in oxygenated ACSF at 35°C. Neurons were visualized using infrared differential interference contrast (IR-DIC) microscopy (Zeiss FS Axioskop, Oberkochen, Germany). DAT-tomato positive cells were identified by switching to epifluorescence using a mercury lamp (X-cite, 120Q, Lumen Dynamics). Up to three cells were patched simultaneously. Borosilicate glass pipettes (Hilgenberg) of 6 - 8 MOhm resistance were pulled with a Flaming / Brown micropipette puller P-1000 (Sutter Instruments). The intracellular solution contained 130 mM K-gluconate, 5 mM KCl, 10 mM HEPES, 4 mM Mg-ATP, 0.3 mM GTP, 10 mM Na2-phosphocreatine (pH 7.25, osmolarity 285 mOsm), 0.2% neurobiotin (Vector laboratories, CA) and Alexa-488 (75 µM) was added to the intracellular solution (Invitrogen). Spontaneous firing was recorded in cell-attached mode before break-in and all other whole-cell recordings were made in current-clamp mode. The intrinsic properties of the neurons were determined by a series of hyperpolarizing and depolarizing current steps and ramps, enabling the extraction of sub- and

365 suprathreshold properties. Recordings were amplified using MultiClamp 700B amplifiers (Molecular
366 Devices, CA, USA), filtered at 2kHz, digitized at 10-20kHz using ITC-18 (HEKA Elektronik, Instrutech, NY,
367 USA), and acquired using custom-made routines running on IgorPro (Wavemetrics, OR, USA). Throughout
368 all recordings pipette capacitance and access resistance were compensated for and data were discarded
369 when access resistance increased beyond 30 MOhm. Liquid junction potential was not corrected for.
370
371 Immunofluorescence
372 Following the recordings, slices were fixated overnight at 4°C in 4% paraformaldehyde solution. Slices were
373 then washed with PBS 1X. For the immunofluorescence, slices were treated with PBS 1X + Triton 0.3% and
374 then incubated with a blocking solution of Normal Serum 10% and Bovine Serum Albumin 1% for 1h at
375 room temperature. Afterward, slices were incubated overnight at 4°C with the following primary
376 antibodies: rabbit anti-TH (Millipore, 1:1000), mouse anti-TPH (Sigma Aldrich, 1:600) and Streptavidin
377 (Jackson Immunoresearch, 1:500). The following day, primary antibodies were washed out and slices were
378 incubated with the appropriate fluorochrome-conjugated secondary antibodies.
379 For the immunostainings in the striatum and SNc and cell counting in DRN, mice were deeply anesthetized
380 and transcardially perfused with PFA 4%. The brains were extracted and post-fixed in PFA 4% for 24 hours.
381 40 um coronal slices were prepared with a vibratome (Leica VT1000 S) and processed as described above.
382
383 Confocal Microscopy Analysis
384 The slices were imaged using Confocal (ZEISS LSM 800) at 10X and 40 X and z-stacks were retrieved. For
385 cell identification, colocalization between neurobiotin and TH or TPH was evaluated.
386
387 Morphological analysis
388 For morphological analysis of dendrites, the confocal z-stacks were used in a semi-manual reconstruction
389 using neuTube [68] and custom code, as previously described [69]. Soma morphology was analyzed by
390 tracing manually the cell body profile, excluding dendritic trunks, in order to measure area (μm^2),
391 perimeter, major and minor axis length (µm) and circularity values. Circularity, calculated as the ratio
392 between the squared perimeter and the area (i.e. $perimeter^2/4\pi$ area), can be a value between 0 and 1 (1
393 for circular shapes and values < 1 for more complex shapes.
394 The morphological analysis was performed on the neurobiotin stacks.
395
396 Western Blot
397 The striata were sonicated in 1% sodium dodecyl sulfate and boiled for 10 min. Equal amounts of protein
398 (25 µg) for each sample were loaded onto 10% polyacrylamide gels and separated by electrophoresis and
399 transferred overnight to nitrocellulose membranes (Thermo Fisher, Stockholm, Sweden). The membranes
400 were immunoblotted with primary antibodies against actin (1:30,000, Sigma Aldrich, Stockholm, Sweden)
401 and TH (1:2000, Millipore, Darmstadt, Germany). Detection was based on fluorescent secondary antibody
402 binding (IR Dye 800CW and 680RD, Li-Cor, Lincoln, NE, USA) and quantified using a Li-Cor Odyssey infrared
403 fluorescent detection system (Li-Cor, Lincoln, NE, USA). The TH protein levels were normalized for the
404 amount of the corresponding actin detected in the sample and then expressed as a percentage of the
405 control (Sham-lesion).
406

Statistical Analysis

Statistical analysis of morphology data was performed using GraphPad Prism 9.2.0. Data are reported as average as ± SEM and analyzed by unpaired t-test. N indicates the number of mice, while n indicates the number of cells. Significance was set at $p<0.05$.

Acknowledgments

We thank Elin Dahlberg for technical assistance and Kristoffer Tenebro Berglund for taking care of the mice. We also thank the members of the Silberberg and Fisone labs and the AND-PD consortium members for comments and discussions.

Funding

This work was supported by a Wallenberg Fellowship from the Knut & Alice Wallenberg Foundation (KAW 2017.0273), the Swedish Brain Foundation (Hjärnfonden, FO2021-0333), and the Swedish Medical Research Council (VR-M, 2019-0 1254) to GS, and a Swedish Research Council International Postdoc Grant (2020-06365) to YJ. RT, RA, GF, and GS are supported by an EU grant (H2020 848002 AND-PD).

Author contributions

Conceptualization: LB, YJ, RT, RM, GF, GS.
Investigation: YJ (electrophysiology, clustering analysis), LB (6-OHDA lesions, morphological analysis, cell counting, western blot).
Visualization: YJ (electrophysiological and clustering results), LB (6-OHDA model, morphological reconstructions).
Supervision: GS and GF.
Writing—original draft: YJ and LB.
Writing—review & editing: LB, YJ, GF, GS.

Competing Interests

The authors declare that they have no competing interests.

Data availability

All raw data is available upon reasonable request.

440 # Figure Legends

441

442 **Figure 1. DRN^{DA} and $DRN^{5\text{-}HT}$ are electrophysiologically distinct cell-types. (A)** Scheme of the location of the DRN (pink)
443 in a coronal section (top) and at higher magnification together with two patch pipettes (center). Bottom: A
444 representative slice stained post recording for TPH, TH and neurobiotin revealing serotonergic neurons (arrows). The
445 ventricle is indicated with a dashed line. **(B)** Top: Differential interference contrast (DIC) microscopy image (left) of
446 neurons that were filled with Alexa488 (right) and neurobiotin. Center, bottom: Staining of the same neurons
447 revealing a TPH-positive ($DRN^{5\text{-}HT}$) neuron and a TPH- and TH-negative cell. **(C)** Top: DIC image of recorded neurons
448 that were filled with Alexa488 and neurobiotin. Center, bottom: Staining of the same neurons revealing tdTomato-
449 and TH-positive (DRN^{DA}) neurons. **(D)** Representative fluorescent (top), DIC (center) image and overlay (bottom) of a
450 tdTomato-positive neuron in a DAT-tdTomato mouse. **(E)** Representative recordings depicting postinhibitory
451 hypoexcitability, slowly ramping currents and rebound oscillations in DRN^{DA} neurons. **(F)** Representative voltage
452 responses to current injections in a TPH-positive ($DRN^{5\text{-}HT}$) and TH-positive (DRN^{DA}) neuron. **(G)** Ramping current
453 injections reveal action potential (AP) amplitude accommodation. Grey circles indicate the onset and peak of APs. **(H)**
454 Amplitude and duration of the AP and action potential afterhyperpolarization (AHP) in a $DRN^{5\text{-}HT}$ and DRN^{DA} neurons.
455 Grey circles indicate onset, peak, and end of the AP and AHP. **(I)** Quantification of electrophysiological properties
456 distinguishing $DRN^{5\text{-}HT}$ from DRN^{DA} neurons (n= 28-43 cells per group, N = 9; Wilcoxon Rank Sum Test). **(J)** Principal
457 component analysis (PCA) of five electrophysiological parameters (insert) and hierarchical cluster analysis based on
458 PCA1 and PCA2 (Ward's method, Euclidean distance). Intrinsic properties were sufficient to separate TPH-positive
459 cells (blue dash) from TH-positive (red dash) cells. Bottom dashes indicate wild type (black) and DAT-tdTomato (gray)
460 mice. Data are shown as mean ± SEM, ***$p < 0.001$. Scale bars: A, 100 µm; B-D, 10 µm.

461

462 **Figure 2. DRN^{DA} and $DRN^{5\text{-}HT}$ have distinct morphological profiles. (A)** Top: representative digital reconstruction of a
463 $DRN^{5\text{-}HT}$ from a wild-type mouse. Bottom: representative digital reconstruction of a DRN^{DA} from a wild-type mouse.
464 Scale bar: 10 µm. **(B-F)** Morphological parameters describing the soma size and shape of $DRN^{5\text{-}HT}$ and DRN^{DA} neurons
465 in Sham-lesion mice ($DRN^{5\text{-}HT}$: n = 20, N = 3; DRN^{DA}: n = 27, N = 3; unpaired t-test). **(G-J)** Morphological parameters
466 describing the dendritic tree of $DRN^{5\text{-}HT}$ and DRN^{DA} neurons in Sham-lesion mice ($DRN^{5\text{-}HT}$: n = 8, N = 3; DRN^{DA}: n = 7, N
467 = 3; unpaired t-test). Data are shown as mean ± SEM, ***$p < 0.001$.

468

469 **Figure 3. Lesions targeting primarily nigrostriatal dopamine increase the excitability of $DRN^{5\text{-}HT}$ neurons whereas loss**
470 **of NA affects their action potentials. (A)** Top: Pie charts showing the number of spontaneously active (dark) and silent
471 (pale) $DRN^{5\text{-}HT}$ neurons in three conditions: Sham (left), 6-OHDA-injected mice (center) and 6-OHDA-injected mice pre-
472 treated with desipramine (DMI + 6-OHDA, right). Bottom: Representative recordings of spontaneously active $DRN^{5\text{-}HT}$
473 neurons (I = 0 pA). **(B)** Quantification of the rheobase (left), the firing frequency of spontaneously active cells (center),
474 and the resting membrane potential of silent $DRN^{5\text{-}HT}$ neurons (right). **(C)** Representative action potentials (APs) of
475 $DRN^{5\text{-}HT}$ at low (left) and high (right) temporal. Grey circles indicate onset, offset, and peak of the APs as well as the
476 end of the afterhyperpolarization (AHP). **(D)** Quantification of the amplitude (left) and duration (right) of the APs of
477 $DRN^{5\text{-}HT}$ neurons. **(E)** Same as in (D) for the AHP. **(F)** Representative responses of $DRN^{5\text{-}HT}$ neurons to current steps (I =
478 +75 pA). **(G)** Quantification of firing frequency / injected current. **(H)** Quantification of the delay to the first AP when
479 injected with current eliciting 2Hz firing. **(I)** Quantification of the membrane time constant (tau) of $DRN^{5\text{-}HT}$ neurons
480 (Sham: n = 22 - 32, N = 6 - 7; 6-OHDA: n = 11 - 16, N = 7; DMI + 6-OHDA: n = 18 – 21, N = 4; unpaired t-test). Data are
481 shown as mean ± SEM, * $p < 0.05$, ** $p < 0.01$.

482 **Figure4. Striatal injection of 6-OHDA induced a hypotrophic phenotype in the $DRN^{5\text{-}HT}$, which is prevented by pre-**
483 **treatment with DMI. (A)** Representative digital reconstructions of a $DRN^{5\text{-}HT}$ neuron in three different conditions: Sham
484 (left), 6-OHDA-injected mice (center) and 6-OHDA-injected mice pre-treated with desipramine (right). Scale bar: 10

485 µm **(B)** Representative confocal pictures of soma from DRN5-HT neurons in Sham (top), 6-OHDA-injected mice
486 (center), and 6-OHDA-injected mice pre-treated with desipramine (bottom). Scale bar: 10 µm. **(C-G)** Morphological
487 descriptors of the soma size and shape in $DRN^{5\text{-}HT}$ neurons (Sham: n = 20, N = 4; 6-OHDA: n = 19, N = 4; DMI + 6-OHDA:
488 n = 17, N = 3; unpaired t-test).**(H-K)** Morphological descriptors of the dendritic tree in $DRN^{5\text{-}HT}$ neurons (Sham: n = 8,
489 N = 3, 6-OHDA: n = 6, N = 3: DMI + 6-OHDA: n = 6, N = 2; unpaired t-test). Data are shown as mean ± SEM, ***p<0.001,
490 **p<0.01. Scale bar: 10 µm.
491
492 **Figure 5. Lesions targeting primarily SN dopamine depolarize DRN^{DA} neurons whereas concomitant loss of NA does**
493 **not affect their action potentials. (A)** Top: Pie charts showing the proportion of spontaneously active (dark) and silent
494 (pale) DRN^{DA} neurons in three conditions: Sham (left), 6OHDA-injected mice (center) and 6-OHDA-injected mice pre-
495 treated desipramine (DMI, right). Bottom: Representative recordings of spontaneously active DRN^{DA} (I = 0pA). **(B)**
496 Quantification of the rheobase (left), the firing frequency of spontaneously active (center), and the resting membrane
497 potential of silent DRN^{DA} neurons (right). **(C)** Representative action potentials (APs) of DRN^{DA} at low (left) and high
498 (right) temporal resolution. Grey circles indicate onset, offset, and peak of APs and the end of the
499 afterhyperpolarization (AHP). **(D)** Quantification of the amplitude (left) and duration (right) of the APs of DRN^{DA}
500 neurons. **(E)** Same as in (D) for the AHP. **(F)** Representative responses of DRN^{DA} neurons to current steps (I = 75pA).
501 Grey circles indicate the delay to the first AP. **(G-I)** Quantification of firing frequency / injected current (G), the delay
502 to the first AP when injected with current eliciting 2 Hz firing (H), and the membrane time constant (tau, I) of DRN^{DA}
503 neurons recorded (Sham: n = 43, N = 8; 6-OHDA: n = 29, N = 6; DMI + 6-OHDA: n = 40, N = 6; unpaired t-test). Data
504 are shown as mean ± SEM, * p < 0.05.

505 **Figure6 Striatal injection of 6-OHDA increased soma complexity and branching in DRN^{DA}. (A)** Representative digital
506 reconstructions of a DRN^{DA} neuron in three different conditions: Sham (left), 6-OHDA-injected mice (center) and 6-
507 OHDA-injected mice pre-treated with desipramine (right). **(B)** Representative confocal pictures of soma from DRN^{DA}
508 neurons in Sham (top), 6-OHDA-injected mice (center), and 6-OHDA-injected mice pre-treated with DMI (bottom). **(C-**
509 **G)** Morphological descriptors of the soma size and shape in DRN^{DA} neurons (Sham: n = 27, N = 7, 6-OHDA: n = 16, N =
510 4; DMI + 6-OHDA: n = 31, N = 5; unpaired t-test). **(H-K)** Morphological descriptors of the dendritic tree in DRN^{DA}
511 neurons. (Sham: n = 7, N = 3; 6-OHDA: n = 11, N = 4; DMI + 6-OHDA: n = 7, N = 3; unpaired t-test). Data are shown as
512 mean ± SEM, *p<0.05. Scale bar: 10 µm.
513
514
515

516 ## References
517

518 1. Braak, H., et al., *Staging of brain pathology related to sporadic Parkinson's disease.*
519 Neurobiol Aging, 2003. **24**(2): p. 197-211.
520 2. Jankovic, J., *Parkinson's disease: clinical features and diagnosis.* J Neurol Neurosurg
521 Psychiatry, 2008. **79**(4): p. 368-76.
522 3. Swick, T.J., *Parkinson's disease and sleep/wake disturbances.* Parkinsons Dis, 2012. **2012**:
523 p. 205471.
524 4. Chaudhuri, K.R. and A.H. Schapira, *Non-motor symptoms of Parkinson's disease:*
525 *dopaminergic pathophysiology and treatment.* Lancet Neurol, 2009. **8**(5): p. 464-74.
526 5. Halliday, G.M., et al., *Loss of brainstem serotonin- and substance P-containing neurons in*
527 *Parkinson's disease.* Brain Res, 1990. **510**(1): p. 104-7.
528 6. Halliday, G.M., et al., *Neuropathology of immunohistochemically identified brainstem*
529 *neurons in Parkinson's disease.* Ann Neurol, 1990. **27**(4): p. 373-85.
530 7. Gesi, M., et al., *The role of the locus coeruleus in the development of Parkinson's disease.*
531 Neurosci Biobehav Rev, 2000. **24**(6): p. 655-68.
532 8. Zarow, C., et al., *Neuronal loss is greater in the locus coeruleus than nucleus basalis and*
533 *substantia nigra in Alzheimer and Parkinson diseases.* Arch Neurol, 2003. **60**(3): p. 337-
534 41.
535 9. Huang, K.W., et al., *Molecular and anatomical organization of the dorsal raphe nucleus.*
536 Elife, 2019. **8**.
537 10. Maillet, A., et al., *Serotonergic and Dopaminergic Lesions Underlying Parkinsonian*
538 *Neuropsychiatric Signs.* Mov Disord, 2021.
539 11. Jørgensen, L.M., et al., *Parkinson patients have a presynaptic serotonergic deficit: A*
540 *dynamic deep brain stimulation PET study.* J Cereb Blood Flow Metab, 2021. **41**(8): p.
541 1954-1963.
542 12. Cheshire, P., et al., *Serotonergic markers in Parkinson's disease and levodopa-induced*
543 *dyskinesias.* Mov Disord, 2015. **30**(6): p. 796-804.
544 13. Pifl, C., G. Schingnitz, and O. Hornykiewicz, *Effect of 1-methyl-4-phenyl-1,2,3,6-*
545 *tetrahydropyridine on the regional distribution of brain monoamines in the rhesus*
546 *monkey.* Neuroscience, 1991. **44**(3): p. 591-605.
547 14. Rylander, D., et al., *Maladaptive plasticity of serotonin axon terminals in levodopa-*
548 *induced dyskinesia.* Ann Neurol, 2010. **68**(5): p. 619-28.
549 15. Nayyar, T., et al., *Cortical serotonin and norepinephrine denervation in parkinsonism:*
550 *preferential loss of the beaded serotonin innervation.* Eur J Neurosci, 2009. **30**(2): p. 207-
551 16.
552 16. Taylor, T.N., et al., *Nonmotor symptoms of Parkinson's disease revealed in an animal*
553 *model with reduced monoamine storage capacity.* J Neurosci, 2009. **29**(25): p. 8103-13.
554 17. Karstaedt, P.J., et al., *Unilateral destruction of dopamine pathways increases ipsilateral*
555 *striatal serotonin turnover in rats.* Exp Neurol, 1994. **126**(1): p. 25-30.
556 18. Wilson, H., et al., *Serotonergic dysregulation is linked to sleep problems in Parkinson's*
557 *disease.* Neuroimage Clin, 2018. **18**: p. 630-637.

558 19. Politis, M., et al., *Depressive symptoms in PD correlate with higher 5-HTT binding in raphe*
559 *and limbic structures.* Neurology, 2010. **75**(21): p. 1920-7.
560 20. Kaya, A.H., et al., *Increased electrical and metabolic activity in the dorsal raphe nucleus of*
561 *Parkinsonian rats.* Brain Res, 2008. **1221**: p. 93-7.
562 21. Prinz, A., et al., *Increased excitability in serotonin neurons in the dorsal raphe nucleus in*
563 *the 6-OHDA mouse model of Parkinson's disease.* Exp Neurol, 2013. **248**: p. 236-45.
564 22. Guiard, B.P., et al., *Functional interactions between dopamine, serotonin and*
565 *norepinephrine neurons: an in-vivo electrophysiological study in rats with monoaminergic*
566 *lesions.* Int J Neuropsychopharmacol, 2008. **11**(5): p. 625-39.
567 23. Wenk, G.L., et al., *Behavioral, biochemical, histological, and electrophysiological effects*
568 *of 192 IgG-saporin injections into the basal forebrain of rats.* J Neurosci, 1994. **14**(10): p.
569 5986-95.
570 24. Lu, J., T.C. Jhou, and C.B. Saper, *Identification of wake-active dopaminergic neurons in the*
571 *ventral periaqueductal gray matter.* J Neurosci, 2006. **26**(1): p. 193-202.
572 25. Dzirasa, K., et al., *Dopaminergic control of sleep-wake states.* J Neurosci, 2006. **26**(41): p.
573 10577-89.
574 26. Cho, J.R., et al., *Dorsal Raphe Dopamine Neurons Modulate Arousal and Promote*
575 *Wakefulness by Salient Stimuli.* Neuron, 2017. **94**(6): p. 1205-1219.e8.
576 27. Lin, R., et al., *The Raphe Dopamine System Controls the Expression of Incentive Memory.*
577 Neuron, 2020. **106**(3): p. 498-514.e8.
578 28. Matthews, G.A., et al., *Dorsal Raphe Dopamine Neurons Represent the Experience of*
579 *Social Isolation.* Cell, 2016. **164**(4): p. 617-31.
580 29. Taylor, N.E., et al., *The Role of Glutamatergic and Dopaminergic Neurons in the*
581 *Periaqueductal Gray/Dorsal Raphe: Separating Analgesia and Anxiety.* eNeuro, 2019.
582 **6**(1).
583 30. Li, C., et al., *Mu Opioid Receptor Modulation of Dopamine Neurons in the Periaqueductal*
584 *Gray/Dorsal Raphe: A Role in Regulation of Pain.* Neuropsychopharmacology, 2016. **41**(8):
585 p. 2122-32.
586 31. Flores, J.A., et al., *Opiate anti-nociception is attenuated following lesion of large dopamine*
587 *neurons of the periaqueductal grey: critical role for D1 (not D2) dopamine receptors.* Pain,
588 2004. **110**(1-2): p. 205-14.
589 32. Flores, J.A., et al., *Role for dopamine neurons of the rostral linear nucleus and*
590 *periaqueductal gray in the rewarding and sensitizing properties of heroin.*
591 Neuropsychopharmacology, 2006. **31**(7): p. 1475-88.
592 33. Dougalis, A.G., et al., *Functional properties of dopamine neurons and co-expression of*
593 *vasoactive intestinal polypeptide in the dorsal raphe nucleus and ventro-lateral*
594 *periaqueductal grey.* Eur J Neurosci, 2012. **36**(10): p. 3322-3332.
595 34. Cardozo Pinto, D.F., et al., *Characterization of transgenic mouse models targeting*
596 *neuromodulatory systems reveals organizational principles of the dorsal raphe.* Nat
597 Commun, 2019. **10**(1): p. 4633.
598 35. Fu, W., et al., *Chemical neuroanatomy of the dorsal raphe nucleus and adjacent structures*
599 *of the mouse brain.* J Comp Neurol, 2010. **518**(17): p. 3464-94.
600 36. Okaty, B.W., et al., *Multi-Scale Molecular Deconstruction of the Serotonin Neuron System.*
601 Neuron, 2015. **88**(4): p. 774-91.

602 37. Lindeberg, J., et al., *Transgenic expression of Cre recombinase from the tyrosine*
603 *hydroxylase locus.* Genesis, 2004. **40**(2): p. 67-73.
604 38. Lammel, S., et al., *Diversity of transgenic mouse models for selective targeting of midbrain*
605 *dopamine neurons.* Neuron, 2015. **85**(2): p. 429-38.
606 39. Carter, M.E., et al., *Tuning arousal with optogenetic modulation of locus coeruleus*
607 *neurons.* Nat Neurosci, 2010. **13**(12): p. 1526-33.
608 40. Pudovkina, O.L., T.I. Cremers, and B.H. Westerink, *Regulation of the release of serotonin*
609 *in the dorsal raphe nucleus by alpha1 and alpha2 adrenoceptors.* Synapse, 2003. **50**(1): p.
610 77-82.
611 41. Trulson, M.E. and T. Crisp, *Role of norepinephrine in regulating the activity of serotonin-*
612 *containing dorsal raphe neurons.* Life Sci, 1984. **35**(5): p. 511-5.
613 42. Haddjeri, N., C. de Montigny, and P. Blier, *Modulation of the firing activity of*
614 *noradrenergic neurones in the rat locus coeruleus by the 5-hydroxtryptamine system.* Br J
615 Pharmacol, 1997. **120**(5): p. 865-75.
616 43. Singewald, N., et al., *Influence of excitatory amino acids on basal and sensory stimuli-*
617 *induced release of 5-HT in the locus coeruleus.* Br J Pharmacol, 1998. **123**(4): p. 746-52.
618 44. Aston-Jones, G., et al., *Serotonin selectively attenuates glutamate-evoked activation of*
619 *noradrenergic locus coeruleus neurons.* J Neurosci, 1991. **11**(3): p. 760-9.
620 45. Lammel, S., et al., *Unique properties of mesoprefrontal neurons within a dual*
621 *mesocorticolimbic dopamine system.* Neuron, 2008. **57**(5): p. 760-73.
622 46. Neuhoff, H., et al., *I(h) channels contribute to the different functional properties of*
623 *identified dopaminergic subpopulations in the midbrain.* J Neurosci, 2002. **22**(4): p. 1290-
624 302.
625 47. Bonito-Oliva, A., D. Masini, and G. Fisone, *A mouse model of non-motor symptoms in*
626 *Parkinson's disease: focus on pharmacological interventions targeting affective*
627 *dysfunctions.* Front Behav Neurosci, 2014. **8**: p. 290.
628 48. Bonito-Oliva, A., et al., *Cognitive impairment and dentate gyrus synaptic dysfunction in*
629 *experimental parkinsonism.* Biol Psychiatry, 2014. **75**(9): p. 701-10.
630 49. Strickland, J.A. and M.A. McDannald, *Brainstem networks construct threat probability and*
631 *prediction error from neuronal building blocks.* Nat Commun, 2022. **13**(1): p. 6192.
632 50. Hajós, M., et al., *Neurochemical identification of stereotypic burst-firing neurons in the rat*
633 *dorsal raphe nucleus using juxtacellular labelling methods.* Eur J Neurosci, 2007. **25**(1): p.
634 119-26.
635 51. Schweimer, J.V., et al., *Spike-timing relationship of neurochemically-identified dorsal*
636 *raphe neurons during cortical slow oscillations.* Neuroscience, 2011. **196**(4): p. 115-23.
637 52. Dahlstroem, A. and K. Fuxe, *EVIDENCE FOR THE EXISTENCE OF MONOAMINE-*
638 *CONTAINING NEURONS IN THE CENTRAL NERVOUS SYSTEM. I. DEMONSTRATION OF*
639 *MONOAMINES IN THE CELL BODIES OF BRAIN STEM NEURONS.* Acta Physiol Scand Suppl,
640 1964: p. Suppl 232:1-55.
641 53. Pollak Dorocic, I., et al., *A whole-brain atlas of inputs to serotonergic neurons of the dorsal*
642 *and median raphe nuclei.* Neuron, 2014. **83**(3): p. 663-78.
643 54. Weissbourd, B., et al., *Presynaptic partners of dorsal raphe serotonergic and GABAergic*
644 *neurons.* Neuron, 2014. **83**(3): p. 645-62.

55. Gocho, Y., et al., *Electrophysiological and pharmacological properties of GABAergic cells in the dorsal raphe nucleus.* J Physiol Sci, 2013. **63**(2): p. 147-54.
56. Xu, Z., et al., *Whole-brain connectivity atlas of glutamatergic and GABAergic neurons in the mouse dorsal and median raphe nuclei.* Elife, 2021. **10**.
57. Bowker, R.M., et al., *Descending serotonergic, peptidergic and cholinergic pathways from the raphe nuclei: a multiple transmitter complex.* Brain Res, 1983. **288**(1-2): p. 33-48.
58. Rivera, H.M. and C.L. Bethea, *Ovarian steroids increase PSD-95 expression and dendritic spines in the dorsal raphe of ovariectomized macaques.* Synapse, 2013. **67**(12): p. 897-908.
59. Park, M.R., *Intracellular horseradish peroxidase labeling of rapidly firing dorsal raphe projection neurons.* Brain Res, 1987. **402**(1): p. 117-30.
60. Calizo, L.H., et al., *Raphe serotonin neurons are not homogenous: electrophysiological, morphological and neurochemical evidence.* Neuropharmacology, 2011. **61**(3): p. 524-43.
61. Diaz-Cintra, S., et al., *Nucleus raphe dorsalis: a morphometric Golgi study in rats of three age groups.* Brain Res, 1981. **207**(1): p. 1-16.
62. Li, Y.Q., et al., *Morphological features and electrophysiological properties of serotonergic and non-serotonergic projection neurons in the dorsal raphe nucleus. An intracellular recording and labeling study in rat brain slices.* Brain Res, 2001. **900**(1): p. 110-8.
63. Kamińska, K., et al., *Depressive-like neurochemical and behavioral markers of Parkinson's disease after 6-OHDA administered unilaterally to the rat medial forebrain bundle.* Pharmacol Rep, 2017. **69**(5): p. 985-994.
64. Fulceri, F., et al., *Nigrostriatal damage with 6-OHDA: validation of routinely applied procedures.* Ann N Y Acad Sci, 2006. **1074**: p. 344-8.
65. Wang, S., et al., *Unilateral lesion of the nigrostriatal pathway induces an increase of neuronal firing of the midbrain raphe nuclei 5-HT neurons and a decrease of their response to 5-HT(1A) receptor stimulation in the rat.* Neuroscience, 2009. **159**(2): p. 850-61.
66. Mei, J., E. Muller, and S. Ramaswamy, *Informing deep neural networks by multiscale principles of neuromodulatory systems.* Trends Neurosci, 2022. **45**(3): p. 237-250.
67. Masini, D., et al., *A Guide to the Generation of a 6-Hydroxydopamine Mouse Model of Parkinson's Disease for the Study of Non-Motor Symptoms.* Biomedicines, 2021. **9**(6).
68. Feng, L., T. Zhao, and J. Kim, *neuTube 1.0: A New Design for Efficient Neuron Reconstruction Software Based on the SWC Format.* eNeuro, 2015. **2**(1).
69. Hjorth, J.J.J., et al., *The microcircuits of striatum in silico.* Proc Natl Acad Sci U S A, 2020. **117**(17): p. 9554-9565.

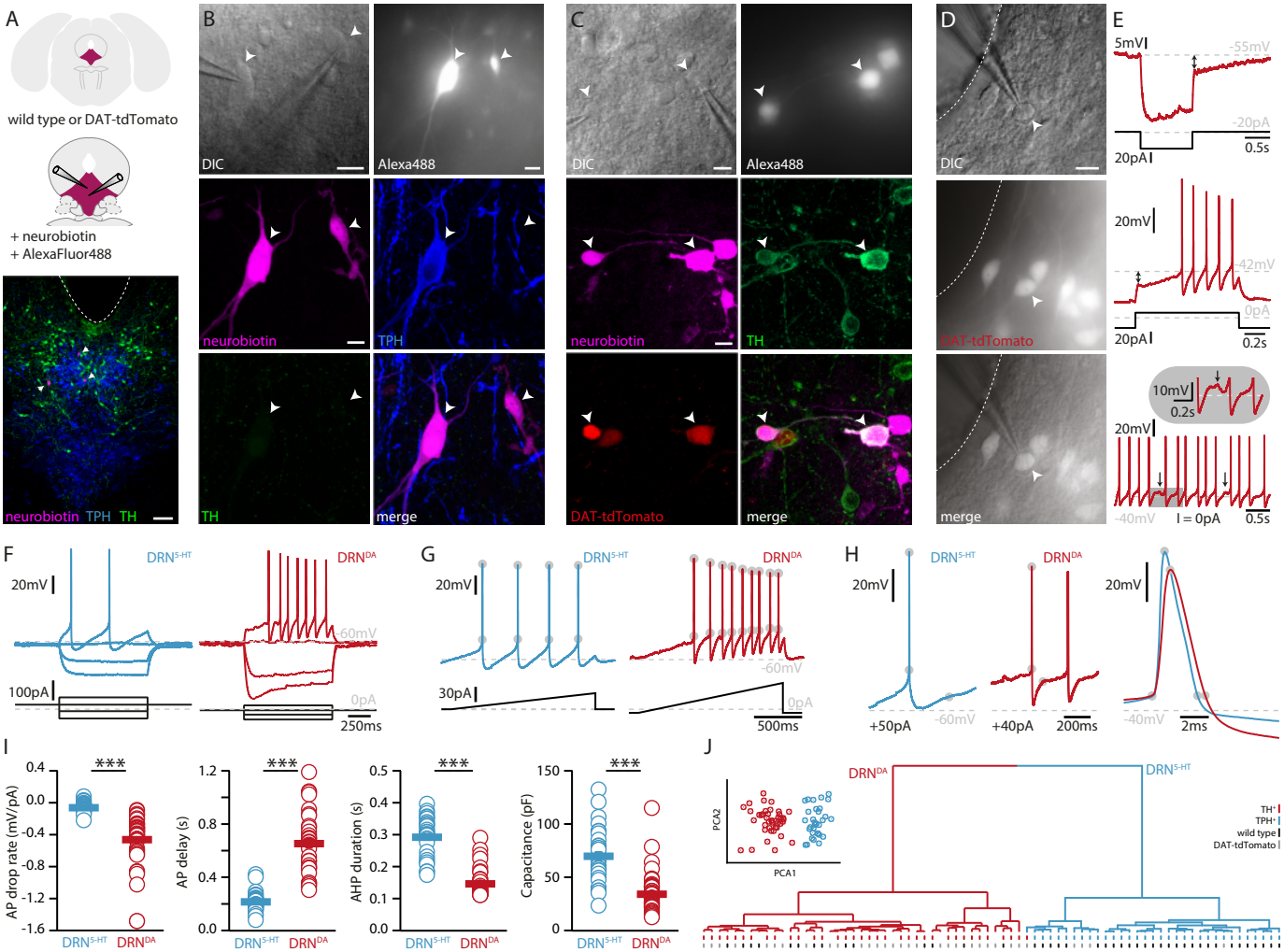
A
wild type or DAT-tdTomato
+ neurobiotin
+ AlexaFluor488
neurobiotin TPH TH
B
DIC
Alexa488
neurobiotin
TPH
TH
merge
C
DIC
Alexa488
neurobiotin
TH
DAT-tdTomato
merge
D
DIC
DAT-tdTomato
merge
E
5mV
-55mV
-20pA
20pA
0.5s
20mV
42mV
0pA
20pA
0.2s
10mV
0.2s
20mV
-40mV
I = 0pA
0.5s
F
DRN5-HT
DRNDA
20mV
100pA
-60mV
0pA
250ms
G
DRN5-HT
DRNDA
20mV
30pA
-60mV
0pA
500ms
H
DRN5-HT
DRNDA
20mV
+50pA
-60mV
+40pA
200ms
-40mV
2ms
I
AP drop rate (mV/pA)
AP delay (s)
AHP duration (s)
Capacitance (pF)
***
DRN5-HT
DRNDA
J
DRNDA
DRN5-HT
PCA2
PCA1
TH+
TPH+
wild type
DAT-tdTomato

Fig. 1

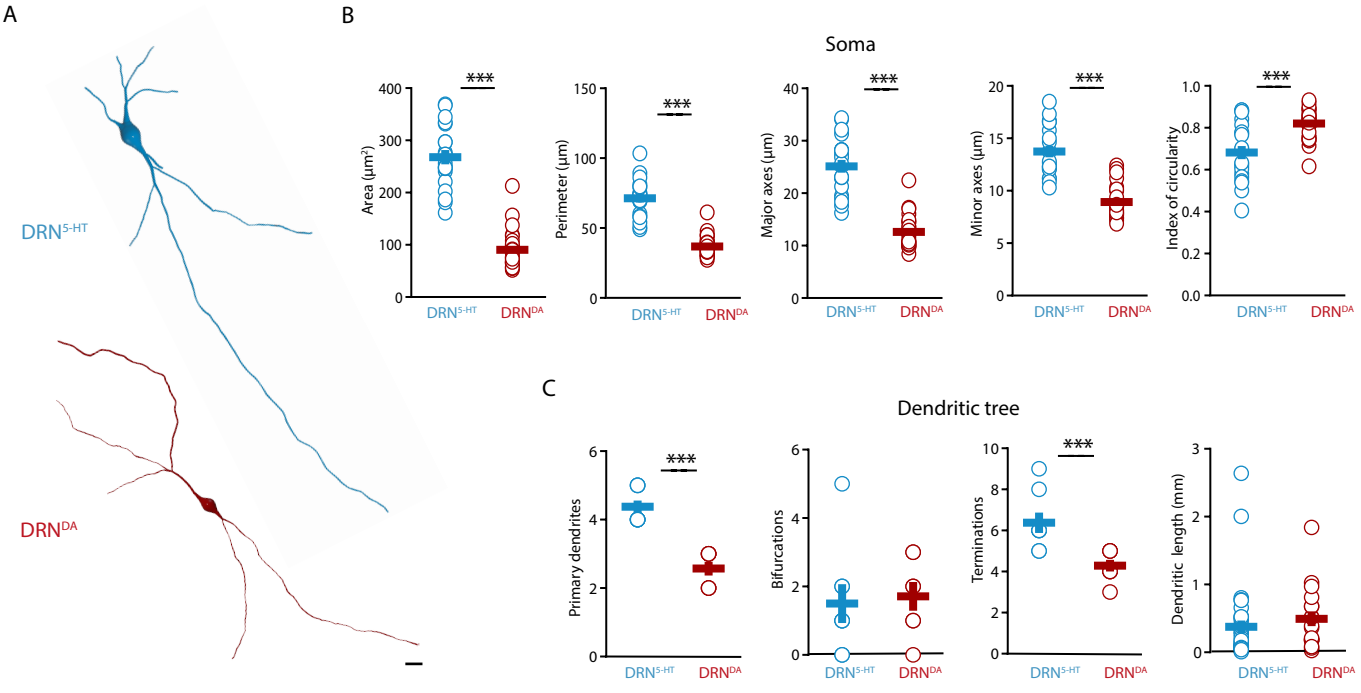
A
DRN5-HT
DRNDA
B
Soma
Area (µm²)
Perimeter (µm)
Major axes (µm)
Minor axes (µm)
Index of circularity
***
DRN5-HT
DRNDA
C
Dendritic tree
Primary dendrites
Bifurcations
Terminations
Dendritic length (mm)

Fig. 2

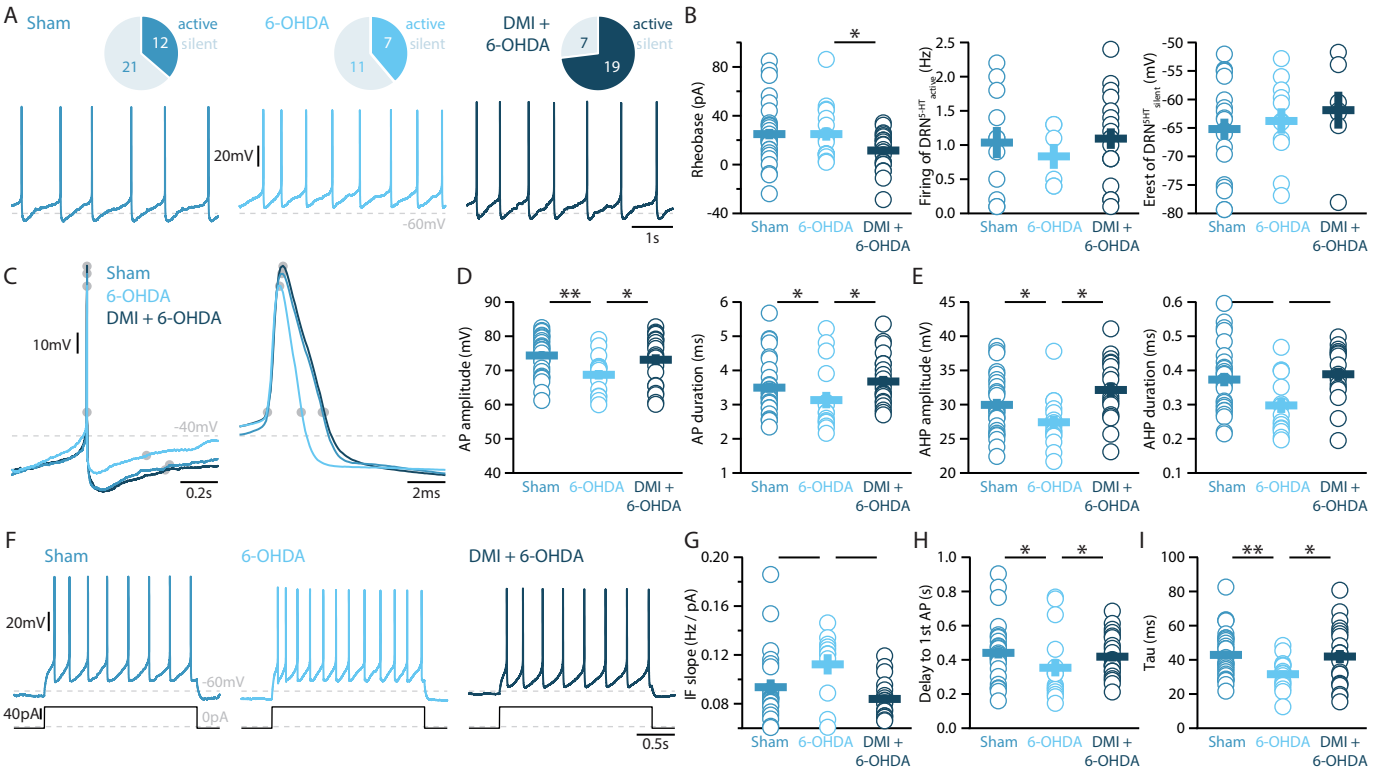
A
Sham
active
silent
12
21
6-OHDA
7
11
DMI + 6-OHDA
19
20mV
-60mV
1s
B
Rheobase (pA)
Firing of DRN5-HT active (Hz)
Erest of DRN5HT silent (mV)
Sham
6-OHDA
DMI + 6-OHDA
C
10mV
-40mV
0.2s
2ms
D
AP amplitude (mV)
AP duration (ms)
E
AHP amplitude (mV)
AHP duration (ms)
F
40pA
0pA
0.5s
G
IF slope (Hz / pA)
H
Delay to 1st AP (s)
I
Tau (ms)

Fig. 3

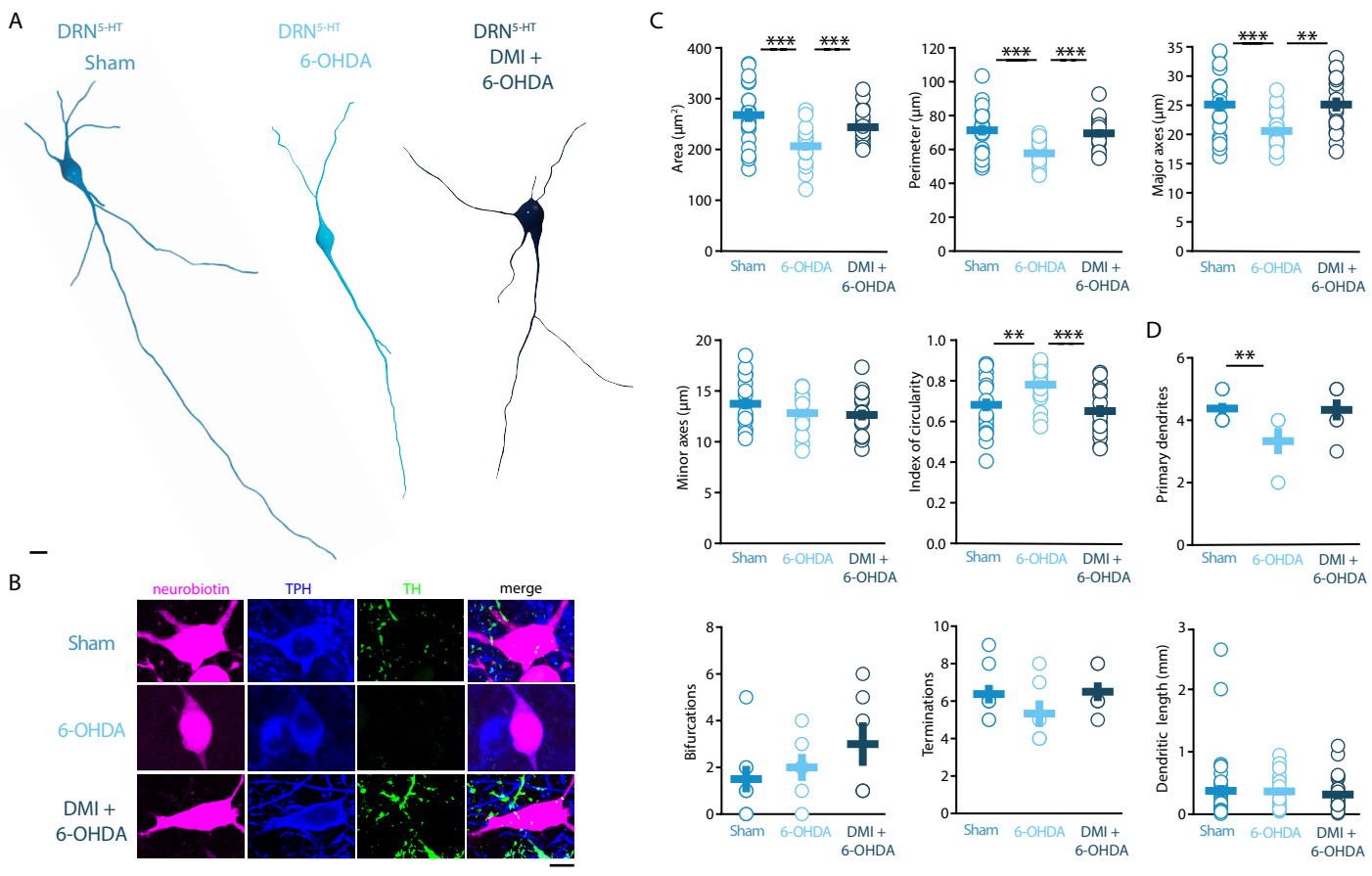
A
DRN5-HT
Sham
DRN5-HT
6-OHDA
DRN5-HT
DMI +
6-OHDA
B
neurobiotin
TPH
TH
merge
Sham
6-OHDA
DMI +
6-OHDA
C
Area (µm²)
Perimeter (µm)
Major axes (µm)
Minor axes (µm)
Index of circularity
Bifurcations
Terminations
Dendritic length (mm)
Sham
6-OHDA
DMI +
6-OHDA
D
Primary dendrites

Fig. 4

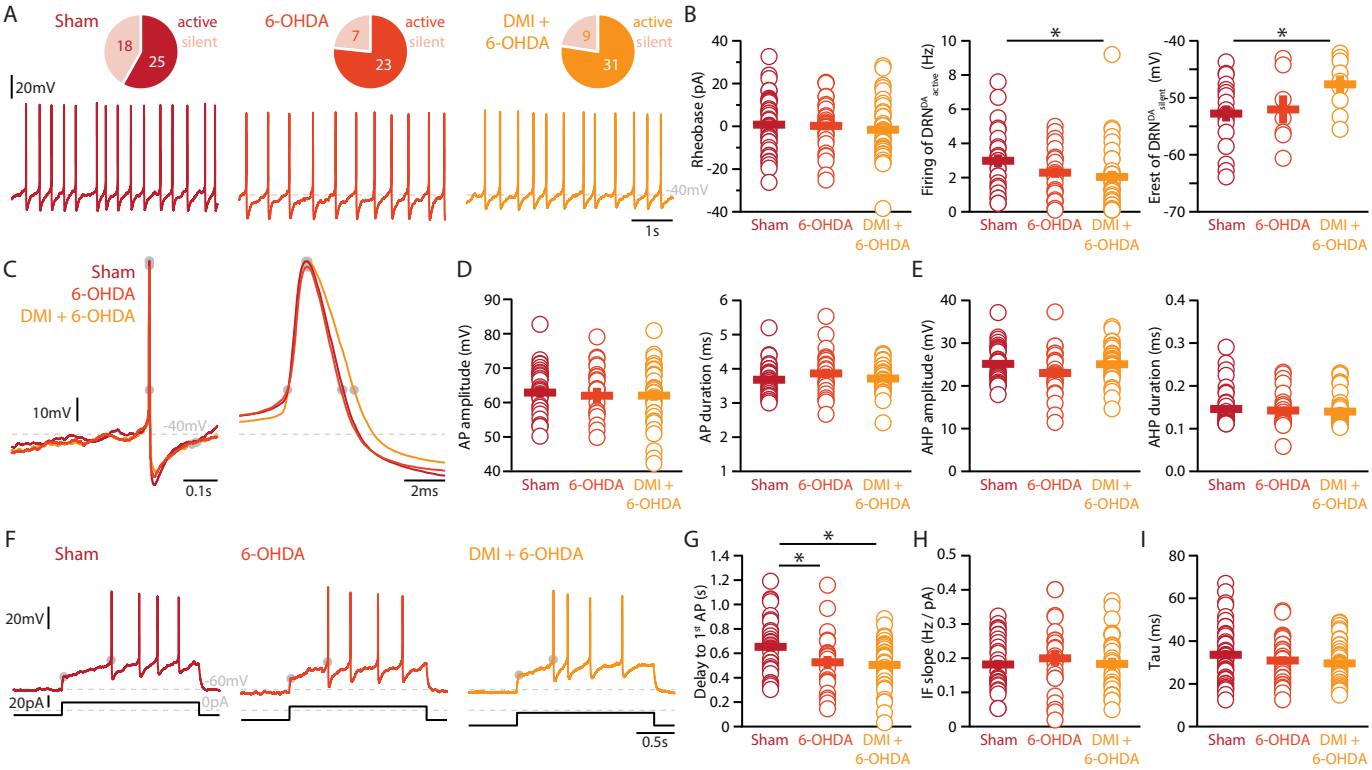
A
Sham
active
silent
18
25
6-OHDA
7
23
DMI + 6-OHDA
9
31
20mV
-40mV
1s
B
Rheobase (pA)
Firing of DRN^DA active (Hz)
Erest of DRN^DA silent (mV)
Sham
6-OHDA
DMI + 6-OHDA
C
Sham
6-OHDA
DMI + 6-OHDA
10mV
-40mV
0.1s
2ms
D
AP amplitude (mV)
AP duration (ms)
E
AHP amplitude (mV)
AHP duration (ms)
F
Sham
6-OHDA
DMI + 6-OHDA
20mV
-60mV
20pA
0pA
0.5s
G
Delay to 1st AP (s)
H
IF slope (Hz / pA)
I
Tau (ms)

Fig. 5

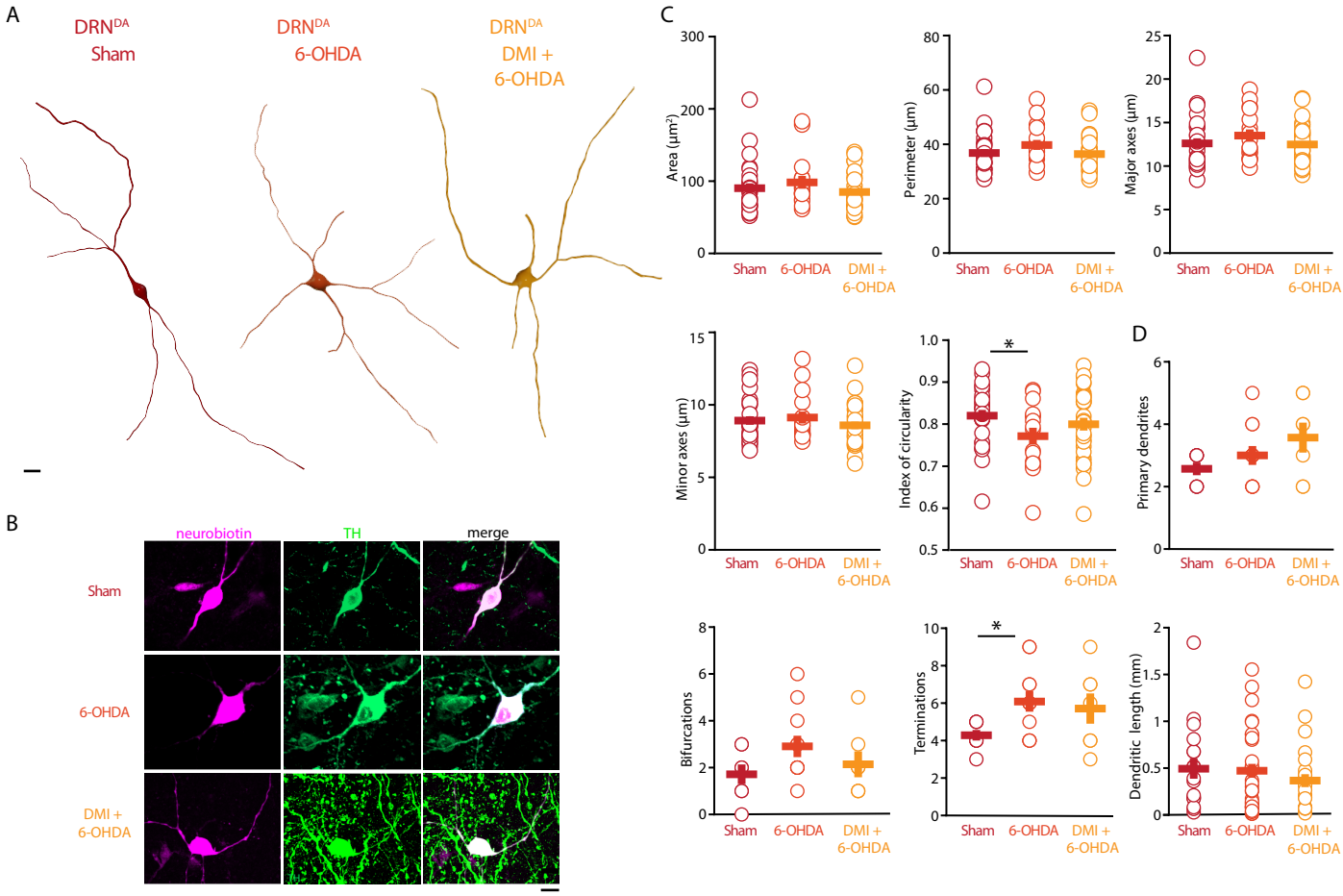
A
DRN^DA Sham
DRN^DA 6-OHDA
DRN^DA DMI + 6-OHDA
B
neurobiotin
TH
merge
Sham
6-OHDA
DMI + 6-OHDA
C
Area (µm²)
Perimeter (µm)
Major axes (µm)
Minor axes (µm)
Index of circularity
Primary dendrites
Bifurcations
Terminations
Dendritic length (mm)
Sham
6-OHDA
DMI + 6-OHDA
*
D

Fig. 6